Geochemistry Geophysics Geosystems G3

Published by AGU and the Geochemical Society

Research Letter
Volume 13, Number 3
8 March 2012
Q03006, doi:10.1029/2011GC003988
ISSN: 1525-2027

The influence of deformation history on the interpretation of seismic anisotropy

Philip Skemer
Department of Earth and Planetary Sciences, Washington University in Saint Louis, 1 Brookings Drive, Box 1169, Saint Louis, Missouri 63130, USA (pskemer@wustl.edu)

Jessica M. Warren
Department of Geological and Environmental Sciences, Stanford University, 450 Serra Mall, Stanford, California 94305, USA

Greg Hirth
Department of Geological Sciences, Brown University, 324 Brook Street, Box 1846, Providence, Rhode Island 02912, USA

[1] Seismic anisotropy in the mantle is primarily caused by the lattice-preferred orientation (LPO) of olivine, which forms and evolves in response to progressive plastic deformation. The style of LPO and its rate of evolution depend on the effects of physical and chemical conditions on the microphysics of deformation and recovery. Here, we integrate results from laboratory experiments and naturally deformed shear zones to evaluate how variability in the evolution of olivine LPO modifies existing strategies for interpreting seismic anisotropy. We concentrate on two particular effects. First, we show that olivine A- and E-type LPOs evolve with opposite senses of rotation, producing a wide spectrum of angular relationships between the orientation of fast seismic wave propagation and the direction of flow. Second, we show that the presence of a pre-existing LPO introduces a lag between changes in deformation kinematics and alignment of the seismic fast direction with the shear direction. The combination of these two factors affects the inference of deformation kinematics from seismic anisotropy and the interpretation of shear wave splitting parameters.

Components: 6100 words, 5 figures.

Keywords: mantle; olivine; seismic anisotropy.

Index Terms: 3902 Mineral Physics: Creep and deformation; 5112 Physical Properties of Rocks: Microstructure; 7208 Seismology: Mantle (1212, 1213, 8124).

Received 29 November 2011; **Revised** 2 February 2012; **Accepted** 4 February 2012; **Published** 8 March 2012.

Skemer, P., J. M. Warren, and G. Hirth (2012), The influence of deformation history on the interpretation of seismic anisotropy, *Geochem. Geophys. Geosyst.*, *13*, Q03006, doi:10.1029/2011GC003988.

1. Introduction

[2] An important objective of geophysics is the determination of flow patterns in Earth's mantle. These kinematics are mostly inferred from seismic anisotropy. However, seismology cannot directly image deformation. Rather, seismology detects the presence of elastically anisotropic structures. Assumptions about the relationships between these structures and kinematics are needed to infer

patterns of flow [*Kaminski and Ribe*, 2002; *Karato et al.*, 2008]. The objective of this study is to highlight important details of the evolution of olivine LPO, and evaluate their significance to the interpretation of seismic anisotropy.

[3] Typically, it is assumed that most seismic anisotropy in the upper mantle is caused by the crystallographic alignment, or LPO, of olivine, which has a strong intrinsic elastic anisotropy [*Mainprice and Silver*, 1993; *Nicolas and Christensen*, 1987]. In olivine, the fastest P wave velocities, and under many conditions the fast S-wave polarizations, are parallel to the [100] crystallographic axis. Analyses of naturally deformed peridotite demonstrate that that when olivine deforms by dislocation creep its [100] crystallographic axes often cluster close to the sample lineation. The sample lineation is, in turn, typically inferred to be sub-parallel to the direction of shear [*Ben Ismail and Mainprice*, 1998; *Nicolas and Christensen*, 1987]. Thus, to a first order, seismic anisotropy is assumed to be closely linked to the direction of shear, or more generally to the kinematics of deformation. These observations are reinforced by some laboratory experiments, which demonstrate that olivine [100] axes cluster and rotate into the shear plane/direction at relatively small strains ($\gamma < 1.5$) [*Bystricky et al.*, 2000; *Nicolas et al.*, 1973; *Zhang and Karato*, 1995; *Zhang et al.*, 2000]. This behavior has been reproduced in numerical models of LPO evolution, which are calibrated using these and other experimental results [*Kaminski and Ribe*, 2001; *Tommasi et al.*, 2000; *Wenk and Tomé*, 1999]. The inferred relationship between deformation kinematics and seismic anisotropy has been widely used to interpret seismological data [e.g., *Long and Becker*, 2010; *Long and Silver*, 2008; *Savage*, 1999; *Wiens et al.*, 2008] and to construct forward models for the formation of anisotropy in a convecting mantle [*Becker et al.*, 2006a, 2003, 2006b; *Blackman and Kendall*, 2002; *Conrad et al.*, 2007; *Hall et al.*, 2000; *Lassak et al.*, 2006; *Tommasi*, 1998].

[4] The basic relationships between deformation kinematics and LPO are well understood, particularly when deformation and microstructure are inferred to be at steady state. However, a number of additional factors must be considered in complicated dynamic settings, where the conditions of deformation continuously evolve [*Castelnau et al.*, 2009; *Chastel et al.*, 1993; *Kaminski and Ribe*, 2002]. The evolution of olivine LPO is controlled by the feedbacks between plastic deformation and consequent microstructures [*Kaminski and Ribe*, 2001; *Karato*, 1987; 1988; *Lee et al.*, 2002; *Wenk and Tomé*, 1999]. Deformation and microstructure interact in a variety of ways, depending on the physical and chemical conditions and integrated history of deformation. Reviews of LPO development are presented by *Karato* [2008], *Kocks et al.* [2000], and *Wenk* [1985, and references therein]. In this contribution, we highlight two effects that are important to the interpretation of observed seismic anisotropy and to the prediction of seismic anisotropy through geodynamic modeling. First, we discuss the relationship between anisotropy and strain for the different types of LPO. Second, we discuss the influence of strain history on LPO evolution. Finally, we present some illustrative calculations to demonstrate the influence of these effects on shear wave splitting.

2. Influence of Different Fabric Types

[5] Laboratory experiments show that a variety of distinct olivine LPOs form at different deformation conditions [*Jung and Karato*, 2001; *Jung et al.*, 2006; *Katayama et al.*, 2004]. These LPOs, referred to as A- through E-type, have characteristic orientations with respect to the kinematics of deformation when inferred to be at steady state. Thus each has a unique seismic signature. These LPO types have been used to interpret many seismological observations in geodynamic contexts [*Karato et al.*, 2008]. As illustrated in Figure 1, some of the different olivine LPO types also exhibit dramatically different evolution patterns as a function of strain. Following previous studies [*Warren et al.*, 2008; *Zhang and Karato*, 1995], we plot (ϕ) – defined as the angle between the densest cluster of olivine [100] axes and the direction of shear – to convey the obliquity between the seismic signature and the kinematics of deformation. This analysis is relevant only for LPOs that form in a simple shear geometry, under dry, or modest water contents, and involve deformation on one of the [100](0kl) slip systems. These LPOs are known as A, E, or D-type fabrics [*Jung et al.*, 2006] (Figure 2) and represent the majority of samples found in nature [*Ben Ismail and Mainprice*, 1998; *Nicolas et al.*, 1971; *Tommasi et al.*, 2000]. Because all of these LPO types involve deformation on one or more of the [100] slip systems, all are predicted to produce anisotropy with the fast direction subparallel to shear. When symmetry about the [100] axis is assumed, the seismic signatures of these LPO types are very similar [*Chevrot and van der Hilst*, 2003].

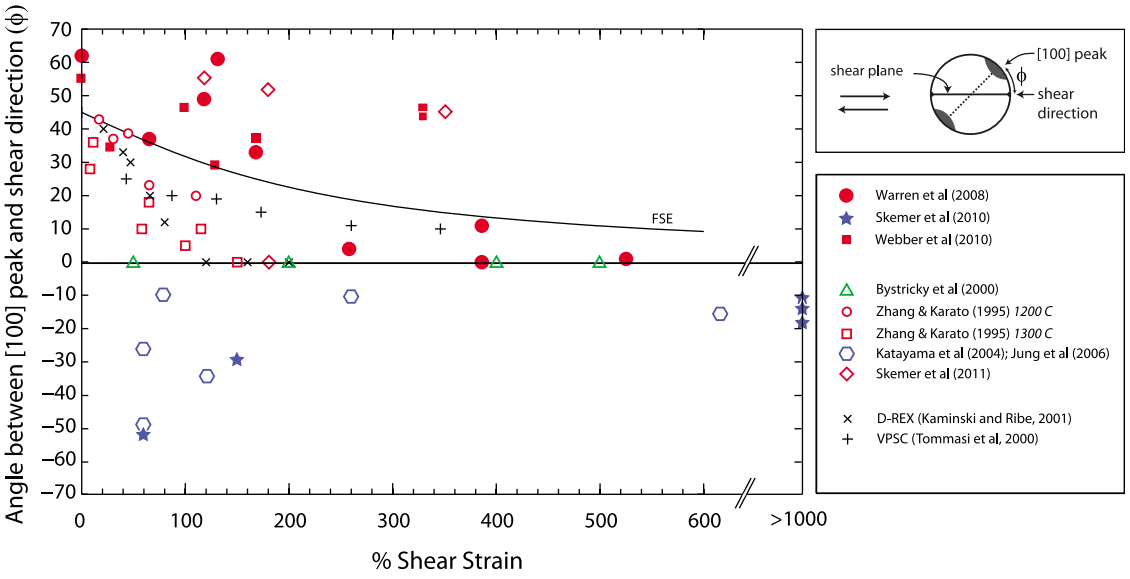

Figure 1. A compilation of data showing the relationship between olivine LPO and shear strain in experiments, numerical models, and naturally deformed samples, which deformed on one of the [100](0kl) slip systems in dextral simple shear. (ϕ) represents the angle between the densest cluster of olivine [100] axes and the shear plane/shear direction. Positive values indicate that the [100] peak is located anticlockwise from the shear direction for dextral shear. When data fall on the black line representing $\phi = 0$, this indicates that the seismic anisotropy is coincident with the shear direction. Data that do not fall on this line have a seismic signature that is oblique to the shear direction. Filled symbols are naturally deformed samples, open symbols are experimental samples, and other symbols are numerical models. Red data are interpreted as olivine A-type fabrics, green data as olivine D-type fabrics, and blue data as olivine E-type fabrics.

[6] Experimental studies that produce A-type fabrics, inferred to result from dominant slip on the [100](010) slip system [*Zhang and Karato*, 1995] (Figure 2), show that with increasing strain the [100] axes rotate in the same sense as the long axis of the finite strain ellipsoid (FSE). However, unlike the FSE, the [100] axes quickly approach the shear direction (Figure 1). Numerical models of LPO evolution predict the same sense of rotation [*Kaminski and Ribe*, 2001; *Ribe and Yu*, 1991;

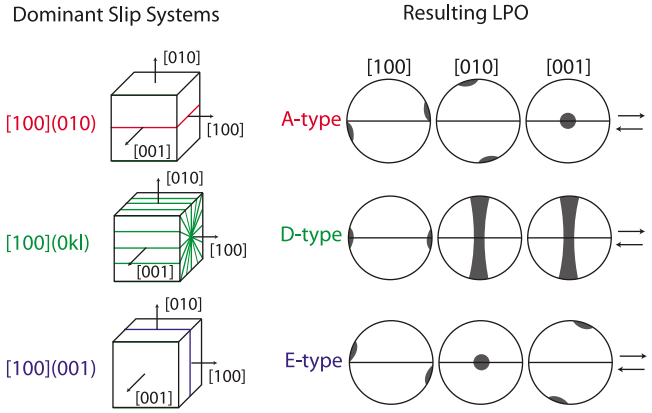

Figure 2. Three of the dominant slip systems for olivine, as well as the resulting LPO formed by deformation in simple shear [*Karato et al.*, 2008]. (left) Dominant slip systems, with colored lines denoting the slip plane or planes. While all three slip systems involve slip in the [100] direction, the set of slip planes are distinct. (right) Cartoon simplifications of resulting LPOs. These pole figures are drawn for right lateral shear (top to the right shear sense) with the shear direction oriented EW and the pole to the shear plane oriented NS. Grey shapes indicate the expected orientations of clustered crystallographic data. A and E-type fabrics have orthorhombic symmetry. D-type fabrics have crystallographic data in girdles, often referred to as hexagonal symmetry. Obliquity of the A- and E-type LPO with respect to the shear direction is illustrated schematically.

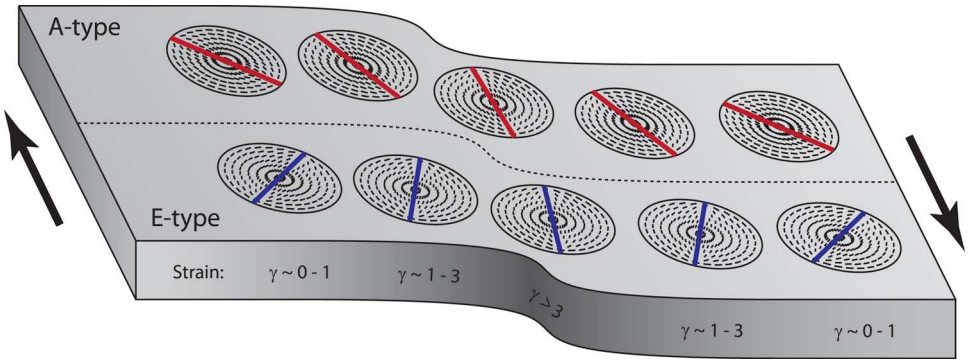

Figure 3. Schematic model of a transverse shear zone with a gradient in shear strain (γ) from the exterior to the center. The polarization of fast shear waves are plotted in a lower hemisphere stereonet projection for (top) A-type and (bottom) E-type fabrics [*Mainprice*, 1990]. Small hatch marks show the orientation of the fast shear wave for a range of back-azimuth and incidence angles. The long lines show the orientation of the fast shear wave for a vertically incident shear wave. The obliquity between the polarization of vertically incident shear waves and the shear zone itself is dependent on the type of olivine fabric that produces that anisotropy and the magnitude of strain.

Tommasi et al., 2000; *Wenk et al.*, 1991]. Geological observations from kinematically constrained mantle shear zones also show this sense of LPO rotation, demonstrating that some extrapolation from laboratory to geological strain rates is valid [*Warren et al.*, 2008; *Webber et al.*, 2010].

[7] E-type fabrics, which form at slightly larger water contents than A-type fabrics, primarily involve activation of the [100](001) slip system (Figure 2). Importantly, experiments by *Katayama et al.* [2004], the first to produce the E-type LPO, show that the sense of rotation of the [100] axes is opposite to that of the FSE long axis. The authors interpreted this to be a result of complementary slip system activity, for example slip on the [001](100) system. Recently, we have confirmed this experimental observation with additional data from kinematically constrained mantle shear zones [*Skemer et al.*, 2010]. The similarity between laboratory and natural samples indicate that finite strain and the physical and chemical environment, rather than strain rate or stress, are the most important considerations when evaluating the evolution of LPO. This consistency also reinforces the efficacy of experimental approaches to study microstructural evolution in olivine, despite large extrapolations in strain rate.

[8] For E-type LPOs, the counter-rotation of [100] axes with respect to the vorticity of simple shear means that values for ϕ are negative (Figure 1). This has a number of consequences for the interpretation of seismic anisotropy. First, as noted by *Katayama et al.* [2004], care must be taken in the interpretation of shear sense from the obliquity of LPO or the dip of an anisotropic layer, as the apparent shear sense will be reversed if the anisotropy is caused by an E-type LPO (Figure 3). Second, the distribution of potential angular relationships between seismic anisotropy and kinematics is broader than would be expected if only A-type fabrics were formed. Indeed, for samples with low shear strain ($\gamma < 1$), there is roughly 90 degrees separating the [100] axis orientations of some A-type fabrics and E-type fabrics, bracketing the direction of shear. As a consequence, there may be large uncertainty in the interpretation of the fastest seismic velocities in terms of kinematics. With increasing strain this uncertainty decreases, as both the A- and E-type [100] axes rotate toward the shear direction, reducing the spectrum of possible kinematic orientations inferred from seismic data. However, as we demonstrate below, under some conditions the alignment of the seismically fast [100] axes with the shear direction may require larger strains than typically assumed.

3. Influence of Pre-existing Fabrics

[9] When deformation kinematics change, LPO will evolve as well. However, modifying a pre-existing LPO is not as straightforward as forming an LPO from a randomly distributed microstructure. Many laboratory experiments on olivine use hot isostatic pressed (HIP) aggregates as their starting material, including the studies by *Bystricky et al.* [2000] and *Zhang and Karato* [1995]. These HIP samples are typically very fined grained ($d < 50\ \mu m$) and exhibit nearly random initial preferred orientation. In these studies, the olivine [100] axes cluster and rotate into the shear plane at relatively

small strains ($\gamma < 1.5$, Figure 1). Notably, the strain required to rotate into the shear plane depends on temperature [*Zhang and Karato*, 1995]. The experiments of *Zhang and Karato* [1995], particularly those at 1300°C, show that olivine [100] axes rotate into the shear plane at significantly smaller strains than the FSE. However, the experiments at 1200°C show less dynamic recrystallization and slower rotation of the [100] axes (Figure 1). This variability over a relatively narrow range of experimental conditions highlights the sensitivity of LPO evolution to temperature-dependent microphysical processes.

[10] In laboratory deformation experiments on coarse-grained natural starting materials with a pre-existing LPO, evolution of the LPO is observed to require larger strain than HIP aggregates [*Skemer et al.*, 2011]. Complementary observations from natural shear zones, which all have pre-existing LPOs, also demonstrate that LPO evolution in geologic settings require considerably larger strains (Figure 1). A study by *Warren et al.* [2008] on a 60 m wide shear zone through the Josephine Peridotite (SW Oregon) found that strains of $\gamma > 2.5$ are required to bring the olivine [100] axes into concordance with the shear direction. Another study by *Webber et al.* [2010] on centimeter scale shear zones in the Red Hills (New Zealand) suggested that still larger strains ($\gamma > 3.3$) may be required under some conditions. *Skemer et al.* [2010] identified E-type LPO in a different shear zone through the Josephine Peridotite. In this case, significant obliquity between the olivine [100] axis and the shear direction was observed at shear strains of $\gamma > 10$. Given the magnitude of strain, we suggest that this obliquity is a steady state feature. Pre-existing fabrics have also been interpreted to modify the ultimate steady state LPO pattern during later stage deformation events [*Michibayashi and Mainprice*, 2004; *Toy et al.*, 2008].

[11] The lag in the reorientation of LPO within natural shear zones may be attributable to several competing effects, including a pre-existing fabric, the amount of orthopyroxene, the initial grain-size, deformation temperature, and other factors that influence the rate and style of dynamic recrystallization. In spite of these potential complications, the general consistency in the sense of rotation between natural and experimental samples indicates that LPO evolution is not significantly influenced by strain rate. While more laboratory experiments are needed to determine the sensitivity of LPO evolution to various microphysical processes, it is clear that under many geological circumstances, microstructure may lag significantly behind evolving kinematics.

4. Modeling

[12] When shear is horizontal and strain is confined to two dimensions, the lag between LPO and deformation kinematics is represented by the dip of the [100] axes, as shown in Figure 1. More complex deformation histories or activity of the [100](001) slip system may also introduce dip of the [001] axes. To illustrate how this might manifest itself in shear wave splitting data, we have used the forward modeling software SynthSplit [*Abt and Fischer*, 2008] to calculate shear wave splitting parameters for some simple cases. The objective here is to simulate only the variation in shear wave splitting parameters due to the two microstructural effects described above. Therefore, we consider only vertically incident waves traversing a single homogeneous layer. By making these two simplifications, we eliminate the dependence of shear wave splitting parameters on the back-azimuth and on the polarization of the incoming wave, both of which have been studied in detail by other groups [*Levin et al.*, 1999; *Rümpker and Silver*, 1998; *Savage*, 1999; *Silver and Savage*, 1994].

[13] Normalized delay times, and deviations in the polarization of the fast axis from the horizontal projection of the [100] axis azimuth are illustrated in Figure 4. For all models we use elastic constants for natural olivine aggregates that were determined by averaging the fabric strength of 110 samples from various dynamic settings [*Ben Ismail and Mainprice*, 1998]. Like most natural samples, the LPO and consequent anisotropy have orthorhombic symmetry. We vary the orientation of two axes: the dip of the a-axis from horizontal (θ), and the rotation of the c-axis about the a-axis (ψ). We use a nominal layer thickness of 50 km and hold the strength of the LPO constant. All delay times are normalized by the maximum delay time in the model, so the choice of layer thickness and LPO strength are unimportant. The initial polarization of the wave is 45 degrees East of North. We do not calculate any model node where the polarization direction is parallel to an axis of crystal symmetry.

[14] When [001] axes are horizontal, as is the case for horizontal shear with an A-type fabric, the delay times vary as a function of [100] axis dip. With increasing [100] dip, the delay time decreases nearly monotonically. When the [100] axis dips by

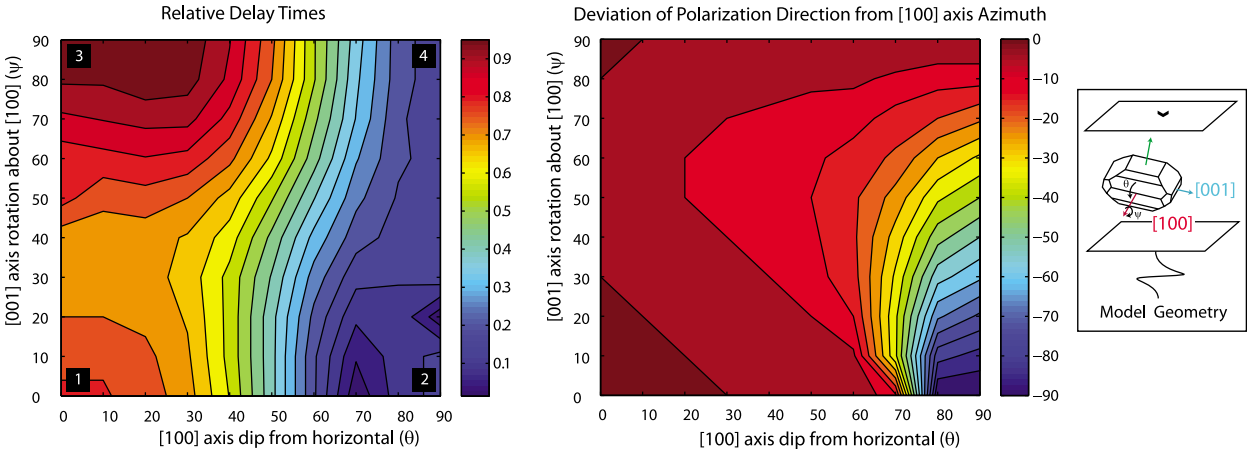

Figure 4. Calculations of synthetic shear wave splitting parameters for an average olivine polycrystal [*Ben Ismail and Mainprice*, 1998] assuming a vertically incident shear wave (see inset for model geometry). (left) Calculated delay times normalized by the maximum model delay time. (right) The angular deviation of the polarization direction from the horizontal projection of the [100] axis orientation. The X-axes show the dip of the [100] axis from horizontal (θ); the Y-axes show the rotation of the [001] axis with respect to the [100] axis (ψ). For olivine LPO with orthorhombic symmetry, rotations beyond 90 degrees are redundant. A [001] axis rotation of zero corresponds to the olivine A-type fabric. Corners labeled 1 and 2 correspond to horizontally and vertically oriented A-type fabrics, respectively. The [001] axis rotated 90 about [100] approximates an olivine E-type fabric. Corners labeled 3 and 4 correspond to horizontally and vertically oriented E-type fabrics, respectively. A range of intermediate dips may be produced by inherited fabrics or complex strain fields.

more than 70 degrees, vertical waves travel subparallel to the [100] axis and are more sensitive to the differences in shear velocities of the [010] and [001] axes. Since shear waves propagate faster parallel to [001] than [010], the orientation of the fast polarization direction will rotate toward the [001] axes. However, delay times for splitting between the [010] and [001] axes are extremely small and so there is a sharp drop in the magnitude of shear wave splitting when [100] axes are steeply dipping.

[15] When the [001] axis is rotated 90 degrees around the [100] axis, a quasi E-type fabric is simulated. In this case, a dipping [100] axis will also produce large variations in delay times. However, little variation in the polarization direction is predicted. For a wide range of intermediate orientations, corresponding to moderately dipping [100] and [001] axes, an assortment of shear wave splitting parameters can be generated. For these intermediate orientations, considerable deviation of the fast direction from the apparent direction of shear is predicted. These types of fabrics are most likely to be found in environments where trench parallel flow, or flow around a slab edge, is superimposed on trench perpendicular corner flow.

[16] In Figure 5, we use the same forward modeling approach to evaluate delay times as a function of strain for the suites of naturally deformed samples shown in Figure 1. For each sample, we use the obliquity of the a-axis with respect to a hypothetically horizontal shear plane as the model input. Again, for consistency, we use the elastic constants for an average olivine sample from *Ben Ismail and Mainprice* [1998]. We also make the assumption that the strength of the LPO is constant, which is supported by the observations of *Warren et al.* [2008]. We assume a homogenous layer 50 km thick that has been sheared horizontally and waves that are vertically incident. While the model's anisotropic layer is much thicker than the shear zones documented in the three studies [*Skemer et al.*, 2010; *Warren et al.*, 2008; *Webber et al.*, 2010] we make the assumption that the relationship between olivine LPO and strain is not length scale dependent. As expected from the general calculation shown in Figure 4, delay times increase with progressive strain, as steeply dipping LPOs are rotated into the horizontal plane. However, over a significant range of strains (0–400%), there is a large variation in the magnitude of the delay times, reflecting the natural variability in LPO orientation.

5. Discussion

[17] Over large length scales and in simple dynamic settings, seismic anisotropy is well correlated with

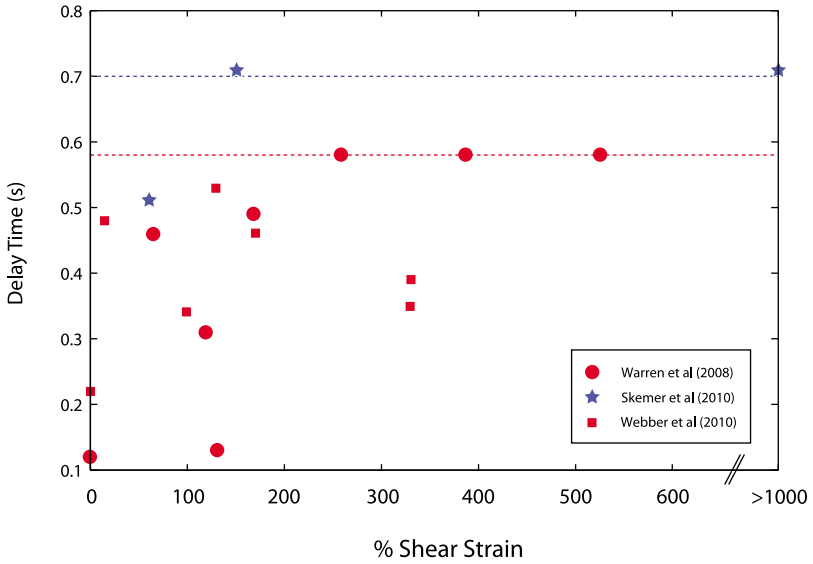

Figure 5. Delay times calculated for naturally deformed peridotites, assuming horizontal shear of a 50 km thick layer, and elastic properties for an average polycrystal from *Ben Ismail and Mainprice* [1998]. Symbols as in Figure 1. Red and blue dashed lines correspond to the delay times for a non-dipping A and E-type LPO, respectively.

plate motions [*Montagner and Tanimoto*, 1991; *Tanimoto and Anderson*, 1984; *Yuan and Romanowicz*, 2010] and global models of mantle strain [*Becker et al.*, 2003]. When calculations of mantle strain are coupled with texturing algorithms, for example D-Rex [*Kaminski et al.*, 2004] or VPSC [*Lebensohn and Tomé*, 1993], these models are in excellent agreement with seismic observations [*Becker et al.*, 2006a; *Conrad et al.*, 2007; *Tommasi*, 1998].

[18] In more complicated settings, for example near plate boundaries, patterns of anisotropy are more difficult to predict and interpret [*Abt et al.*, 2009; *Becker et al.*, 2006b; *Hartog and Schwartz*, 2000; *Kneller et al.*, 2005; *Lassak et al.*, 2006; *Long and Silver*, 2008; *Montagner*, 2002; *Peyton et al.*, 2001; *Pozgay et al.*, 2007; *Smith et al.*, 2001; *Wolfe and Solomon*, 1998]. There are many factors that must be considered in the interpretation of shear wave splitting anisotropy, including the fabric strength [*Mainprice and Silver*, 1993], the depth extent of the anisotropic layer, and the degree of structural heterogeneity [*Rümpker and Silver*, 1998; *Savage*, 1999; *Silver and Savage*, 1994]. Additional consideration of the variability in the relationship between anisotropic microstructures and kinematics may help reconcile some of the differences between plate motions and shear wave splitting in complex tectonic settings [e.g., *Flesch et al.*, 2005; *Holt*, 2000].

[19] In naturally deformed rocks, the presence of a pre-existing LPO produced by evolving kinematics may produce a significant lag between the onset of deformation and the rotation of the LPO into parallelism with the shear direction (Figure 1). Moreover, the physical and chemical conditions of deformation introduce additional uncertainty due to the differences in the sense of rotation of A- and E-type LPOs (Figures 1–3). These two effects must be considered when interpreting seismic anisotropy. As an example, dipping structures can be detected by measuring shear wave splitting from a range of back-azimuths [e.g., *Chevrot and van der Hilst*, 2003]. The standard approach has been to interpret a dipping structure as evidence of shear with horizontal and vertical components. However, if anisotropy lags significantly behind kinematics, horizontal shear could generate an identical dipping structure. Additionally, the relationship between the dipping structure and the sense of the shear will depend on the type of LPO that produces the anisotropy.

[20] To better interpret seismic anisotropy, and implement forward models of seismic anisotropy development, we must be able to predict how LPO evolves as a function of strain and deformation conditions. A key parameter to understand is the lag between the formation/reorientation of LPO and a change in deformation kinematics. If the time scale for LPO reorientation is much longer than the time scale for the change in deformation kinematics, seismic anisotropy generated by olivine LPO cannot be reliably related to the direction of shear [*Kaminski and Ribe*, 2002]. *Kaminski and Ribe*

[2002], using models parameterized by the experimental results of *Zhang and Karato* [1995], suggest that for simple shear the critical time scale for LPO reorientation is approximately $\tau \sim \dot{\varepsilon}^{-1}$. This value is reasonable under some conditions, but may underestimate the time-scale for microstructural evolution in others. We suggest, on the basis of data compiled in Figure 1, that in complex dynamic settings such as mantle wedges, and at particular deformation conditions (for example, low temperatures), the microstructural lag may be several times larger. Expressed in another way, at certain conditions the critical strain for alignment of the seismic fast directions with the shear direction is likely several hundred percent. While the data compiled in this study clearly demonstrate that significant microstructural lag occurs in nature, further study is needed to determine the sensitivity of the microstructural lag to temperature, and other deformation conditions.

6. Conclusions

[21] Laboratory and field studies that describe the formation and evolution of olivine LPO show remarkable similarities, in spite of large differences in strain rate and stress. These data, taken together, illustrate important features that are critical to the interpretation of seismic anisotropy. The different sense of rotation between A- and E-type LPOs will affect the determination of shear sense from seismic data. Deformation history may also introduce lag between changes in deformation kinematics and the alignment of olivine fast axes with the direction of shear. Differences in the evolution of olivine A- and E-type LPOs, compounded by the lag due to pre-existing fabrics, produce a broad spectrum of angular relationships between the orientation of the olivine [100] axis and the direction of shear. Any obliquity between the olivine crystal axes and the inferred kinematics of deformation will affect shear wave splitting parameters. More experimental and theoretical work, and more seismological data in places where kinematics are well-constrained, is needed to understand how olivine LPO evolves and seismic anisotropy is manifested in complex kinematic environments.

Acknowledgments

[22] The authors gratefully thank David Abt and Karen Fischer for providing the SynthSplit software and for assistance with its use. Doug Wiens and Maureen Long are thanked for helpful discussions on the interpretation of seismic anisotropy. Ikuo Katayama is thanked for providing unpublished data on E-type fabrics. Two anonymous reviewers and T. Becker (AE) helped focus the objectives of this paper. This effort was supported by NSF EAR-0911289 and EAR-0738880.

References

Abt, D. L., and K. M. Fischer (2008), Resolving three-dimensional anisotropic structure with shear wave splitting tomography, *Geophys. J. Int.*, *173*, 859–886, doi:10.1111/j.1365-246X.2008.03757.x.

Abt, D. L., K. M. Fischer, G. A. Abers, W. Strauch, J. M. Protti, and V. González (2009), Shear wave anisotropy beneath Nicaragua and Costa Rica: Implications for flow in the mantle wedge, *Geochem. Geophys. Geosyst.*, *10*, Q05S15, doi:10.1029/2009GC002375.

Becker, T. W., et al. (2003), Comparison of azimuthal seismic anisotropy from surface waves and finite strain from global mantle-circulation models, *Geophys. J. Int.*, *155*, 696–714, doi:10.1046/j.1365-246X.2003.02085.x.

Becker, T. W., S. Chevrot, V. Schulte-Pelkum, and D. K. Blackman (2006a), Statistical properties of seismic anisotropy predicted by upper mantle geodynamic models, *J. Geophys. Res.*, *111*, B08309, doi:10.1029/2005JB004095.

Becker, T. W., et al. (2006b), Mantle flow under the western United States from shear wave splitting, *Earth Planet. Sci. Lett.*, *247*, 235–251, doi:10.1016/j.epsl.2006.05.010.

Ben Ismail, W., and D. Mainprice (1998), An olivine fabric database; an overview of upper mantle fabrics and seismic anisotropy, *Tectonophysics*, *296*, 145–157, doi:10.1016/S0040-1951(98)00141-3.

Blackman, D. K., and J. M. Kendall (2002), Seismic anisotropy in the upper mantle: 2. Predictions for current plate boundary flow models, *Geochem. Geophys. Geosyst.*, *3*(9), 8602, doi:10.1029/2001GC000247.

Bystricky, M., et al. (2000), High shear strain of olivine aggregates: Rheological and seismic consequences, *Science*, *290*, 1564–1567, doi:10.1126/science.290.5496.1564.

Castelnau, O., D. K. Blackman, and T. W. Becker (2009), Numerical simulations of texture development and associated rheological anisotropy in regions of complex mantle flow, *Geophys. Res. Lett.*, *36*, L12304, doi:10.1029/2009GL038027.

Chastel, Y. B., P. R. Dawson, H.-R. Wenk, and K. Bennett (1993), Anisotropic convection with implications for the upper mantle, *J. Geophys. Res.*, *98*, 17,757–17,771, doi:10.1029/93JB01161.

Chevrot, S., and R. D. van der Hilst (2003), On the effects of a dipping axis of symmetry on shear wave splitting measurements in a transversely isotropic medium, *Geophys. J. Int.*, *152*, 497–505, doi:10.1046/j.1365-246X.2003.01865.x.

Conrad, C. P., M. D. Behn, and P. G. Silver (2007), Global mantle flow and the development of seismic anisotropy: Differences between the oceanic and continental upper mantle, *J. Geophys. Res.*, *112*, B07317, doi:10.1029/2006JB004608.

Flesch, L. M., et al. (2005), Constraining the extent of crust-mantle coupling in central Asia using GPS, geologic, and shear wave splitting data, *Earth Planet. Sci. Lett.*, *238*, 248–268, doi:10.1016/j.epsl.2005.06.023.

Hall, C. E., K. M. Fischer, E. M. Parmentier, and D. K. Blackman (2000), The influence of plate motion on three-dimensional back arc mantle flow and shear wave splitting, *J. Geophys. Res.*, *105*, 28,009–28,033.

Hartog, R., and S. Y. Schwartz (2000), Subduction-induced strain in the upper mantle east of the Mendocino triple junction, California, *J. Geophys. Res.*, *105*, 7909–7930, doi:10.1029/1999JB900422.

Holt, W. E. (2000), Correlated crust and mantle strain fields in Tibet, *Geology*, *28*, 67–70, doi:10.1130/0091-7613(2000)28<67:CCAMSF>2.0.CO;2.

Jung, H., and S. Karato (2001), Water-induced fabric transitions in olivine, *Science*, *293*, 1460–1463, doi:10.1126/science.1062235.

Jung, H., et al. (2006), Effect of water and stress on the lattice-preferred orientation of olivine, *Tectonophysics*, *421*, 1–22, doi:10.1016/j.tecto.2006.02.011.

Kaminski, E., and N. M. Ribe (2001), A kinematic model for recrystallization and texture development in olivine polycrystals, *Earth Planet. Sci. Lett.*, *189*, 253–267, doi:10.1016/S0012-821X(01)00356-9.

Kaminski, E., and N. M. Ribe (2002), Timescales for the evolution of seismic anisotropy in mantle flow, *Geochem. Geophys. Geosyst.*, *3*(8), 1051, doi:10.1029/2001GC000222.

Kaminski, E., et al. (2004), D-Rex, a program for calculation of seismic anisotropy due to crystal lattice preferred orientation in the convective upper mantle, *Geophys. J. Int.*, *158*, 744–752, doi:10.1111/j.1365-246X.2004.02308.x.

Karato, S. (1987), Seismic anisotropy due to lattice preferred orientation of minerals: Kinematic or dynamic?, in *High-Pressure Research in Mineral Physics*, *Geophys. Monogr. Ser.*, vol. 39, edited by M. H. Manghnani and Y. Syono, pp. 455–471, AGU, Washington, D. C., doi:10.1029/GM039p0455.

Karato, S. (1988), The role of recrystallization in the preferred orientation of olivine, in *Anisotropy and Inhomogeneity of the Lithosphere and Asthenosphere*, edited by V. Babuska et al., pp. 107–122, Elsevier, Amsterdam, Netherlands, doi:10.1016/0031-9201(88)90029-5.

Karato, S. (2008), *Deformation of Earth Materials*, Cambridge Univ. Press, Cambridge, U. K.

Karato, S., et al. (2008), Geodynamic significance of seismic anisotropy of the upper mantle: New insights from laboratory studies, *Annu. Rev. Earth Planet. Sci.*, *36*, 59–95, doi:10.1146/annurev.earth.36.031207.124120.

Katayama, I., et al. (2004), New type of olivine fabric from deformation experiments at modest water content and low stress, *Geology*, *32*, 1045–1048, doi:10.1130/G20805.1.

Kneller, E., et al. (2005), B-type fabric in the mantle wedge: Insights from high-resolution non-Newtonian subduction zone models, *Earth Planet. Sci. Lett.*, *237*, 781–797, doi:10.1016/j.epsl.2005.06.049.

Kocks, U. F., et al. (2000), *Texture and Anisotropy: Preferred Orientations in Polycrystals and Their Effect on Materials*, 692 pp., Cambidge Univ. Press, Cambridge, U. K.

Lassak, T. M., et al. (2006), Seismic characterization of mantle flow in subduction systems: Can we resolve a hydrated mantle wedge?, *Earth Planet. Sci. Lett.*, *243*, 632–649, doi:10.1016/j.epsl.2006.01.022.

Lebensohn, R. A., and C. N. Tomé (1993), A self-consistent anisotropic approach for the simulation of plastic-deformation and texture development of polycrystals: Application to zirconium alloys, *Acta Metall. Mater.*, *41*, 2611–2624, doi:10.1016/0956-7151(93)90130-K.

Lee, K. H., et al. (2002), A scanning electron microscope study of the effects of dynamic recrystallization on lattice preferred orientation in olivine, *Tectonophysics*, *351*, 331–341, doi:10.1016/S0040-1951(02)00250-0.

Levin, V., W. Menke, and J. Park (1999), Shear wave splitting in the Appalachians and the Urals: A case for multilayered anisotropy, *J. Geophys. Res.*, *104*, 17,975–17,993, doi:10.1029/1999JB900168.

Long, M. D., and T. W. Becker (2010), Mantle dynamics and seismic anisotropy, *Earth Planet. Sci. Lett.*, *297*, 341–354, doi:10.1016/j.epsl.2010.06.036.

Long, M. D., and P. G. Silver (2008), The subduction zone flow field from seismic anisotropy: A global view, *Science*, *319*, 315–318, doi:10.1126/science.1150809.

Mainprice, D. (1990), A FORTRAN program to calculate seismic anisotropy from the lattice preferred orientation of minerals, *Comput. Geosci.*, *16*, 385–393, doi:10.1016/0098-3004(90)90072-2.

Mainprice, D., and P. G. Silver (1993), Interpretation of SKS-waves using samples from the subcontinental lithosphere, in *Dynamics of the Subcontinental Mantle: From Seismic Anisotropy to Mountain Building*, edited by D. Mainprice et al., pp. 257–280, Elsevier, Amsterdam, Netherlands, doi:10.1016/0031-9201(93)90160-B.

Michibayashi, K., and D. Mainprice (2004), The role of pre-existing mechanical anisotropy on shear zone development within oceanic mantle lithosphere: An example from the Oman ophiolite, *J. Petrol.*, *45*, 405–414, doi:10.1093/petrology/egg099.

Montagner, J. P. (2002), Upper mantle low anisotropy channels below the Pacific Plate, *Earth Planet. Sci. Lett.*, *202*, 263–274, doi:10.1016/S0012-821X(02)00791-4.

Montagner, J. P., and T. Tanimoto (1991), Global upper mantle tomography of seismic velocities and anisotropies, *J. Geophys. Res.*, *96*, 20,337–20,351, doi:10.1029/91JB01890.

Nicolas, A., and N. I. Christensen (1987), Formation of anisotropy in upper mantle peridotites; a review, in *Composition, Structure and Dynamics of the Lithosphere-Asthenosphere System*, *Geodyn. Ser.*, vol. 16, edited by K. Fuchs and C. Froidevaux, pp. 111–123, AGU, Washington, D. C., doi:10.1029/GD016p0111.

Nicolas, A., et al. (1971), Textures, structures and fabrics due to solid state flow in some European lherzolites, *Tectonophysics*, *12*, 55–86, doi:10.1016/0040-1951(71)90066-7.

Nicolas, A., et al. (1973), Mechanisms of flow in naturally and experimentally deformed peridotites, *Am. J. Sci.*, *273*, 853–876, doi:10.2475/ajs.273.10.853.

Peyton, V., V. Levin, J. Park, M. Brandon, J. Lees, E. Gordeev, and A. Ozerov (2001), Mantle flow at a slab edge: Seismic anisotropy in the Kamchatka region, *Geophys. Res. Lett.*, *28*, 379–382, doi:10.1029/2000GL012200.

Pozgay, S. H., et al. (2007), Complex mantle flow in the Mariana subduction system: Evidence from shear wave splitting, *Geophys. J. Int.*, *170*, 371–386, doi:10.1111/j.1365-246X.2007.03433.x.

Ribe, N. M., and Y. Yu (1991), A theory for plastic deformation and textural evolution of olivine polycrystals, *J. Geophys. Res.*, *96*, 8325–8335, doi:10.1029/90JB02721.

Rümpker, G., and P. G. Silver (1998), Apparent shear-wave splitting parameters in the presence of vertically varying anisotropy, *Geophys. J. Int.*, *135*, 790–800, doi:10.1046/j.1365-246X.1998.00660.x.

Savage, M. K. (1999), Seismic anisotropy and mantle deformation: What have we learned from shear wave splitting?, *Rev. Geophys.*, *37*, 65–106, doi:10.1029/98RG02075.

Silver, P. G., and M. K. Savage (1994), The interpretation of shear-wave splitting parameters in the presence of 2 anisotropic layers, *Geophys. J. Int.*, *119*, 949–963, doi:10.1111/j.1365-246X.1994.tb04027.x.

Skemer, P., et al. (2010), Microstructural and rheological evolution of a mantle shear zone, *J. Petrol.*, *51*, 43–53, doi:10.1093/petrology/egp057.

Skemer, P., et al. (2011), Torsion experiments on coarse-grained dunite: Implications for microstructural evolution when diffusion creep is suppressed, in *Deformation Mechanisms, Rheology and Tectonics: Microstructures, Mechanics and Anisotropy*, *Geol. Soc. Spec. Publ.*, *360*, 211–223.

Smith, G. P., et al. (2001), A complex pattern of mantle flow in the Lau Backarc, *Science*, *292*, 713–716, doi:10.1126/science.1058763.

Tanimoto, T., and D. L. Anderson (1984), Mapping convection in the mantle, *Geophys. Res. Lett.*, *11*, 287–290, doi:10.1029/GL011i004p00287.

Tommasi, A. (1998), Forward modeling of the development of seismic anisotropy in the upper mantle, *Earth Planet. Sci. Lett.*, *160*, 1–13, doi:10.1016/S0012-821X(98)00081-8.

Tommasi, A., D. Mainprice, G. Canova, and Y. Chastel (2000), Viscoplastic self-consistent and equilibrium-based modeling of olivine lattice preferred orientations: Implications for the upper mantle seismic anisotropy, *J. Geophys. Res.*, *105*, 7893–7908, doi:10.1029/1999JB900411.

Toy, V. G., et al. (2008), Quartz fabrics in the Alpine Fault mylonites: Influence of pre-existing preferred orientations on fabric development during progressive uplift, *J. Struct. Geol.*, *30*, 602–621, doi:10.1016/j.jsg.2008.01.001.

Warren, J. M., et al. (2008), Evolution of lattice-preferred orientation during simple shear in the mantle, *Earth Planet. Sci. Lett.*, *272*, 501–512, doi:10.1016/j.epsl.2008.03.063.

Webber, C., et al. (2010), Fabric development in cm-scale shear zones in ultramafic rocks, Red Hills, New Zealand, *Tectonophysics*, *489*, 55–75, doi:10.1016/j.tecto.2010.04.001.

Wenk, H. (1985), *Preferred Orientation in Deformed Metals and Rocks: An Introduction to Modern Texture Analysis*, 610 pp., Academic, Orlando, Fla.

Wenk, H.-R., and C. N. Tomé (1999), Modeling dynamic recrystallization of olivine aggregates deformed in simple shear, *J. Geophys. Res.*, *104*, 25,513–25,527, doi:10.1029/1999JB900261.

Wenk, H.-R., K. Bennett, G. R. Canova, and A. Molinari (1991), Modeling plastic deformation of peridotite with the self-consistent theory, *J. Geophys. Res.*, *96*(B5), 8337–8349, doi:10.1029/91JB00117.

Wiens, D. A., et al. (2008), The seismic structure and dynamics of the mantle wedge, *Annu. Rev. Earth Planet. Sci.*, *36*, 421–455, doi:10.1146/annurev.earth.33.092203.122633.

Wolfe, C. J., and S. C. Solomon (1998), Shear-wave splitting and implications for mantle flow beneath the MELT region of the East Pacific Rise, *Science*, *280*, 1230–1232, doi:10.1126/science.280.5367.1230.

Yuan, H., and B. Romanowicz (2010), Lithospheric layering in the North American craton, *Nature*, *466*, 1063–1068, doi:10.1038/nature09332.

Zhang, S., and S. Karato (1995), Lattice preferred orientation of olivine aggregates deformed in simple shear, *Nature*, *375*, 774–777, doi:10.1038/375774a0.

Zhang, S., et al. (2000), Simple shear deformation of olivine aggregates, *Tectonophysics*, *316*, 133–152, doi:10.1016/S0040-1951(99)00229-2.